Biointerface Research in Applied Chemistry
Open-Access Journal (ISSN: 2069-5837)

Article
Volume 13, Issue 3, 2023, 242
https://doi.org/10.33263/BRIAC133.242

AuNs-GO Nanocomposite Modified Paper-Based Amperometric Biosensor as an Alternative Approach for Early Investigation of Leptospirosis

Vivek Verma [1], Deepak Kala [2], Shagun Gupta [3], Ankur Kaushal [3,*], Dinesh Kumar [1,*]

[1] Shoolini University of Biotechnology and Management Science, Solan-173212, India; vivek77verma@gmail.com; chatantadk@yahoo.com (D.K.)
[2] Department of Biotechnology Engineering, Chandigarh University, Mohali, 140413, India; deepakbiotech90cu@gmail.com (D.K.)
[3] Department of Biotechnology, Maharishi Markandeshwar University, Mullana, Ambala, 134003 India; shagun22_88@yahoo.com (S.G.); ankur.biotech85@gmail.com (A.K.)
* Correspondence: chatantadk@yahoo.com (D.K.); ankur.biotech85@gmail.com (A.K.);

Scopus Author ID 57203256288
Received: 9.03.2022; Accepted: 13.04.2022; Published: 7.06.2022

Abstract: The gold nanoparticles-graphene oxide (AuNs-GO) nanocomposite customized screen-printed paper electrode (AuNs-GO/SPPE) immobilized the *Lipl-41*gene-specific 5'NH_2 labeled single-stranded DNA probe for early diagnosis of leptospirosis using the electrochemical approach. GO nanoparticle was synthesized using the modified hummer's method and reduced chloroauric tetra acid to form gold nanoparticles stabilized graphene oxide (AuNs-GO) nanocomposite. Cyclic voltammetry (CV) and electrochemical impedance spectroscopy (EIS) measured the sensor response after hybridization with ssGDNA of *L. interrogans*. The sensitivity of the developed DNA sensor was calculated as 1487.4 µA/cm^2/ng for ssGDNA of *L. interrogans* using CV studies with a limit of detection (LOD) of 0.002 ng/µl. The nanocomposite was characterized using UV-Vis spectroscopy, Fourier transforms infrared spectroscopy (FTIR), and, Transmission electron microscopy (TEM). The electrode surface modification was also monitored by EIS using potassium-ferricyanide (PBS buffer, 1 mM of pH7.2) as a redox indicator dye. The promising results show that the developed biosensor can become a point-of-need (PON) detection method for the early diagnosis of leptospirosis as it has better sensitivity and specificity, low cost, and rapid response time.

Keywords: DNA biosensor; *Lipl*-41 gene; AuN-GO nanocomposite; screen-printed paper electrode; Leptospirosis.

1. Introduction

Leptospirosis is prevalent in all subtropical and levelheaded areas and is believed to be a prevalent zoonotic contagious in the universe. The disease is caused by a bacterium known as Leptospira (family Leptospiracae) and affects animals and humans. It can cause a broad range of symptoms in humans, a few of which may be inaccurate for other diseases [1]. Because of the diversity of subclinical manifestations seen in leptospirosis, patients at its commencement are usually misdiagnosed with asymptomatic fever or fever (pyrexia) of unknown origin, which later results in multi-organ damage associated with a high mortality rate called 'Weil's syndrome [2]. The disease outbreak was usually associated with sporting events, farmers, tourism, veterinarians, and military personnel [3, 4, 5, 6]. Multiple

conventional diagnosis techniques have been employed for the detection of pathogenic leptospires that include direct investigation of leptospires; serological and molecular diagnosis methods, nevertheless have a variety of limitations, so there is a need to devise a point of the care system to surveil the tendency of the disease to curb its deadly consequences [7, 8, 9, 10]. In the present era, the biosensor-based technique has become excellent equipment for disease diagnosis due to its superior selectivity, sensitivity, specificity, and low response time [11]. Several biosensor techniques, such as tissue-based, enzyme-based, DNA biosensors, immunosensor have significant potential and indispensable uses in disease diagnosis [12, 13, 14,15]. Biosensors can be used in the field of disease diagnostics for the early detection of cardiac disease, cancer, diabetes, and many other contagious diseases [16, 17, 18], which may be a benchmark over the traditional methods. Amperometric biosensors provide a reliable alternative solution to subclinical diagnosis due to their beneficial characteristics, such as higher sensitivity, user-friendly, and better endurance [19]. It creates a point of need (PON) diagnostics facility outside the laboratory services without the help of a trained person. The presentation of the DNA biosensor is extremely dependent on the immobilization of the DNA probe, corresponding to the genes to be investigated, recommended ideal orientation, and order for optimal intent hybridization. The inclusion of some nanomaterials like gold nanoparticles [20,21] and graphene oxide [22, 23,-24] offers stable and well-ordered scaffolding for DNA immobilization onto the working surface of the electrode and can improve the sensitivity of the sensor. Graphene oxide (GO) is a carbon material of a 2-D carbon lattice consisting of carbonyl and hydroxyl groups. It has gained more attention for use in graphene oxide DNA DNA-based sensors by its unique π–π stacking reciprocity [25]. Whereas the functional groups distributed on the GO surface provide an agreeable foundation for molecular bond immobilization of macromolecules by creating an amide bond by its amino group. [26,27]. The capability of DNA immobilization is enhanced by including metal nanoparticles which exhibit great congruence with bio-molecules [28, 29,30]. However, the covalent immobilization of Au nanoparticles with GO acknowledges better resilience and strengthens the electronic competency of one another, and results in increased sensitivity.

In the path of such improvement, a tread was already taken by Nagraik et al. by constructing an amperometric DNA sensor to detect leptospirosis by choosing the highly conserved *LipL-32* gene of *L. interrogans* a genetic marker [31]. The developed sensor was reported with better sensitivity and specificity. Another study showed the *Loa22* gene-based amperometric sensor as an optional technique for the early screening of leptospirosis in terms of sensitivity and specificity [32]. The previously reported biosensors for *L. interrogans* detection were based upon standard glass electrodes or ceramic electrodes and showed some cost, sensitivity, specificity, and response type limitations. The reported approach is based upon the synthesis, and immobilization of different types of nanocomposites onto the surface of the paper electrode to increase the sensor's sensitivity, specificity, and faster response time.

The outer membrane proteins (OMP) that are exposed on the leptospira surface are potentially important in virulence and pathogenesis study due to their position at the interface between the mammalian host and the leptospires [33]. The OMP genes, such as omp*L1*, *lipL32*, *lipL21*, *ligB*, and *LipL-41*, are present in all pathogenic serovars. These genes are found to be highly conserved between different pathogenic *Leptospira* species. Consequently, these genes are helpful in investigating leptospiral infection and act as genetic markers for designing conclusive results in PCR and biosensor applications [34, 35, 36, 37,38]. So, the emphasis of the present study was to construct a *Lipl-41* gene-based DNA sensor for early diagnosis of

leptospirosis with greater selectivity, sensitivity, and specificity using graphene oxide modified gold nanoparticles (AuNs-GO). The sensor was fabricated using SPPE consisting of graphene oxide-modified gold nanoparticles. Furthermore, the electrochemical changes were analyzed by cyclic voltammogram (CV) and impedimetric spectroscopy (EIS).

2. Materials and Methods

2.1. Chemicals.

Tris ethylenediamine-tetraacetic acid, Sodium chloride, Methylene blue, from Qualigens, and ethanol were obtained from Changshu Chemical Co. Ltd. Disodium hydrogen orthophosphate, sodium di-hydrogen orthophosphate, hydrochloric acid, tris-buffered saline (pH 8.0), phosphate-buffered saline (pH 7.2), and other chemicals were procured from Himedia, India. N-hydroxysuccinimide (NHS), 1-ethyl-3-(3-dimethylamino propyl)-carbodiimide (EDC), was purchased from Sigma-Aldrich, USA. Self-designed SPPE (screen-printed paper electrode) were purchased from Class-one System, Saket, New Delhi, and fabricated at Shoolini University, Solan, (H.P.). Bacterial samples were collected and handled at the Postgraduate Institute of Medical Education and Research (PGIMER), Chandigarh. The *Lipl-41*gene-specific amine labeled ssDNAprobe (5′NH2AACGTGCAGACGCAATCAAC-3′) was synthesized from Bio Serve Biotechnology (India) Pvt. Ltd.

2.2. Equipment's.

The surface morphological changes and assemblage of the developed sensor were characterized using UV-Vis spectroscopy, Fourier transforms infrared spectroscopy (FTIR), Dynamic light scattering (DLS), and Field-emission scanning electron microscopy (FE-SEM), respectively. The electrochemical experiments, i.e., cyclic voltammetry (CV) and electrochemical impedance spectroscopy (EIS) were performed using a portable workstation known as Empicostat (DropSens, Spain). The electrochemical study was performed using Potentiostat/Galvanostat of Palmsens software with an SPPE consisting of carbon as a counter and working electrode and silver (AgCl) as a reference electrode.

2.3. Devising of graphene oxide.

The graphene oxide was formulated according to Hummer's method (31). A 15 g of black-lead granules were added to a 20 ml mixture of concentrated sulfuric acid (H_2SO_4), potassium persulfate ($K_2S_2O_8$) (5 g), and phosphorus Oxide (P_2O_5) (4 g). After 8 hours, the blend was allowed to cool at room temperature (RT) and then cautiously mixed with demineralized water and filtered. The obtained yield was precisely cleaned to detach the acid, and certainly, the obtained product is air-dried. A 3 g air-dried yield was then mixed with 50 ml of chilled concentrated sulfuric acid (H_2SO_4). Afterward, 6 g of potassium manganate ($KMnO_4$) was mixed moderately under continuous stirring for 2.5 hours. Subsequently, demineralized water (95 ml) was mixed, and the suspension was allowed to sustain for 15-20 min. The process was accomplished by including demineralized water (270 ml) and 60 ml of 30% hydrogen peroxide solution (H_2O_2). The obtained solution was decanted and washed with 600 ml of 1:10 Hydrogen chloride (HCl) solution. The yellowish-brown yield was then rinsed with demineralized water and air-dried at RT.

2.4. Preparation of AuNs-GO.

From the literature survey (39), 550 µl of GO suspension (0.1%) was mixed with7 ml of demineralized water, followed by adding 600 µl Gold (III) chloride trihydrate $HAuCl_4.3H_2O$ solution (0.1%). The blend was kept for 20 min. at RT under continuous stirring conditions. After, 600 µl of sodium citrate solution (0.002%) was mixed into the blend and stirred at 1000 rpm for 30 min. at 80-85° C. Furthermore; the suspension was centrifuged at 6000 rpm for 15 min. to segregate the sodium citrate solution. The floating liquid on the top was decanted, and the process of removal of the supernatant was continued one more time. At last, 8 ml of Milli-Q water was mixed into the remaining residue to make the AuNs-GO.

2.5.Modification of AuNs-GO/SPPE.

Before electrochemical studies, the SPPE was first washed with ethanol and then with demineralized water and air-dried at RT. The prepared solution of AuNs-GO (1mg) was mixed in 1 ml of demineralized water, and 4 µl of volume was drop-coated onto the working area of SPPE and dried at 35-40°C. Figure 1 represents the fabrication of AuNs-GO-based nanocomposite onto SPPE.

2.6. DNA sensor construction.

To fabricate the DNA sensor (*Lipl-41*-AuNs-GO), the amine-linked capture probe (*Lipl-41*) was immobilized on the customized SPPE (AuNs-GO/SPPE) with the help of 1 mM of EDC: NHS (1:1) for 1.5 hours to activate the carboxyl group for carbodiimide cross-linking. The electrode's working surface was then washed several times using phosphate-buffer saline (PBS, pH 7.2) and dried at RT.

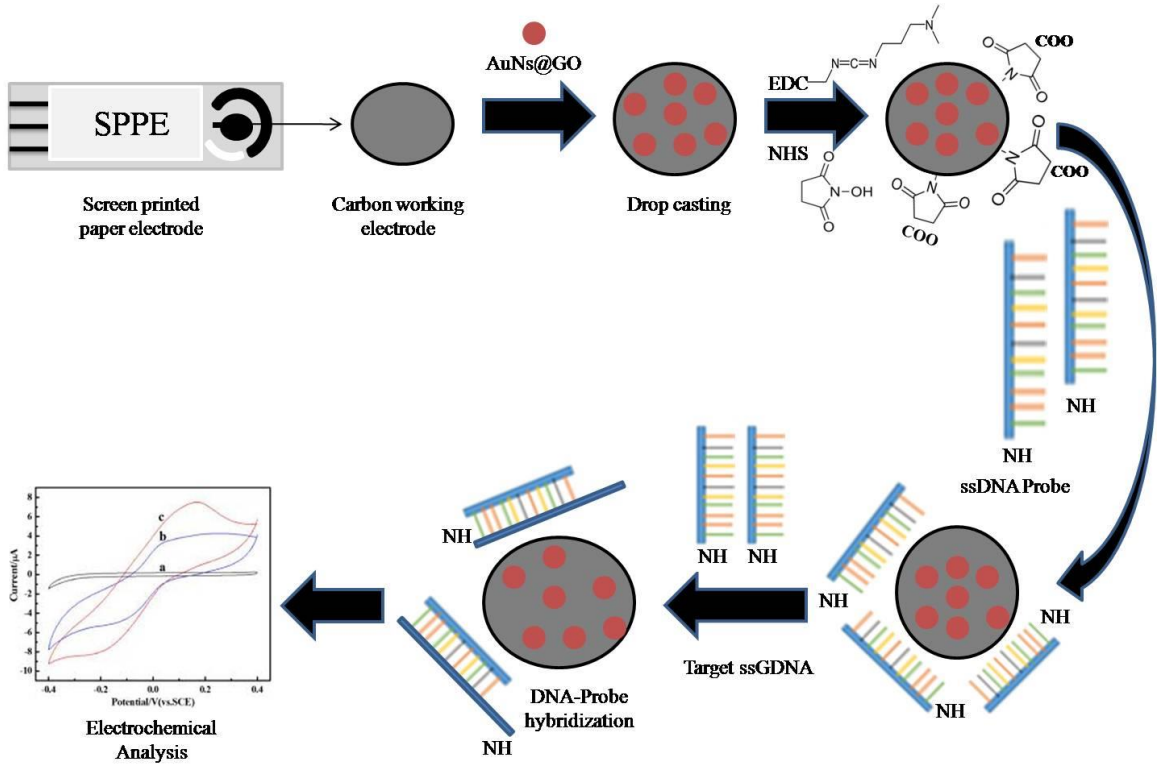

Figure 1. Schematic illustration of AuNs-GO/SPPE electrochemical DNA sensor fabrication process.

The amino linked (5' NH_2) ssDNA probe (3 µl, 10 µM) was added onto the activated working electrode surface (AuNs-GO/CNF) and incubated in a humid chamber for 4 hours.

Further, the ssDNA probe modified electrode (AuNs-GO/c-CNFs/ssDNA $_{probe}$) was washed using TE buffer (pH 8.0) to recapture the excessive probe. The leptospiremic genomic DNA was denatured (95°C, 5 min.) and used for hybridization with the modified electrode (AuNs-GO/CNF/ssDNA probe) for 10 min. at RT. The same course was repeated for hybridization with different concentrations of the *L. interrogans* ssGDNA. The CV analysis was performed with Potentiostat at a potential scan of -1.0 to 0.5 V using methylene blue (PBS, pH-7.2), and impedimetric studies were recorded using 2.5 mM potassium- ferricyanide at a frequency scan of 10^{-2} -10^{5} Hz.

2.7. Specificity and selectivity study.

The specificity of the sensor was achieved using CV to evaluate its ability to differentiate between the targeted DNA sequences (ssGDNA of *L. interrogans*) with other bacterial ssGDNA (*K. pneumoniae, E. coli, S. aureus,* and *O. tsutsugamushi*) to obtain the selectivity. The developed sensor characteristic was assessed at 10 ng/µl of DNA concentration for all microorganisms. The *L. interrogans* is an intracellular domain of human blood corpuscles, so the h-GDNA (human GDNA) was taken as a negative control because the patient's sample contains huge contaminants.

The selectivity of the specific ssDNA probe sequence towards the *Lipl-41* gene was differentiated using a cDNA sequence with a different number of multiple mismatched bases (Table 1). The developed DNA sensor was hybridized with cDNA sequence, different mismatched base sequences, and the relative current (*Ip*) values were recorded concerning the ssDNA probe. The change in *Ip* values concerning ssDNA probe was used for evaluating the selectivity of the ssDNA probe towards the cDNA sequence and with the sequences containing multiple numbers of mismatched bases.

Table 1.The nucleotide sequences of cDNA and mismatched DNA base sequences.

Samples	Mismatch DNA sequences
Complementary DNA	5′GTTGATTGCGTCTGCACGTT 3′
1-BMM	5′ATTGATTGCGTCTGCACGTT 3′
2-BMM	5′AGTGATTGCGTCTGCACGTT 3′
3-BMM	5′AGCGATTGCGTCTGCACGTT 3′
4-BMM	5′AGCCATTGCGTCTGCACGTT 3′
MBMM	5′ACCCCAGAACCTAAGAACACT3′

BMM: Base mismatch, MBMM: multiple Base mismatch

2.8. Validation of DNA sensor.

The developed amperometric DNA sensor was validated using 10 positive patients' blood DNA samples using a CV study. The DNA samples were isolated from the 'patient's sample using DNA isolation Mini Kit (QIAamp) and denatured at 95ºC for 5 min. to make the DNA single-stranded and further subjected to hybridization with an ssDNA probe, and *Ip* values were measured by using CV study. The difference in current values with respect to the ssDNA$_{probe}$, positive control (PCR confirmed *L. interrogans* GDNA), and negative control (Human GDNA) was optimized and further compared in order to validate the patient samples. The concentration of 10ng/µl for all ssGDNA samples was used for hybridization concerning the ssDNA probe. The patient sample used for the validation study was also confirmed using the Microscopic agglutination test (MAT) to examine the results with the available commercial kit.

3. Results and Discussion

3.1. Non-electrochemical characterizations.

3.1.1. Ultraviolet-visible spectroscopy.

The UV-Visible spectrum of the developed nanoparticles was ensured (Figure 2) using UV-Vis spectroscopy. The prepared Au nanoparticles manifest a predictable absorption peak at 531 nm (Fig. 2 A). The absorption peak of Graphene oxide at 250 and 295 nm was allocated to n→π* transits to C=O bonds, and the π→π* transits to C=C were due to the presence of carbonyl groups of GO (40) (Fig. 2 B). The amide connection formed between GO and 4-amino thiophenol diminishes the band severity of the free carboxyl groups present in GO, due to which a weak band pops up at 531 nm.

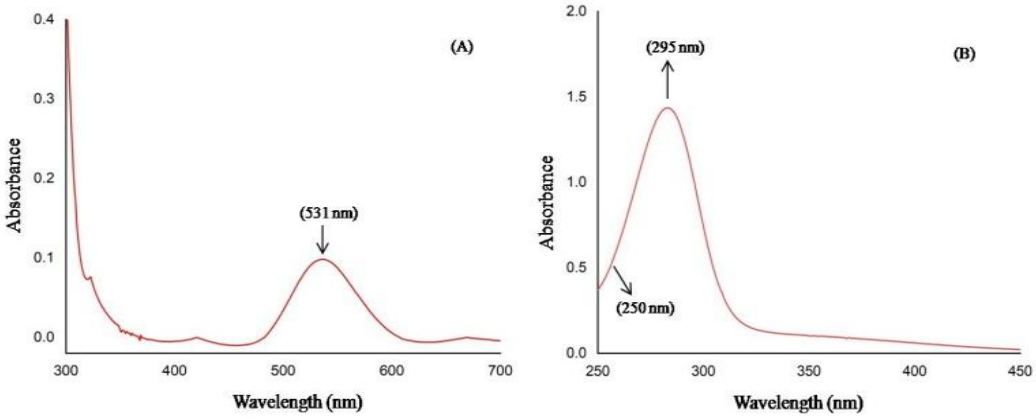

Figure 2. The UV-visible spectrum of the AuNs-GO and GO nanocomposite in a wavelength of 250 to 700 nm.

3.1.2. FTIR (Fourier-Transform Infrared Spectroscopy).

The observed FTIR spectrum shows a nice gesture of achieving the construction procedure. The FTIR spectra show an acute and broad peak in Figure 3 (A) (AuNs-GO) at 3401 cm^{-1} representing the O-H groups of carbonyl/carboxyl acid in Figure 3 (B) GOpeaks at 1640, 1408, and 855 cm^{-1} attributes to C=C, C=O, and aromatic C-O groups indicate the presence of GO [41-43].

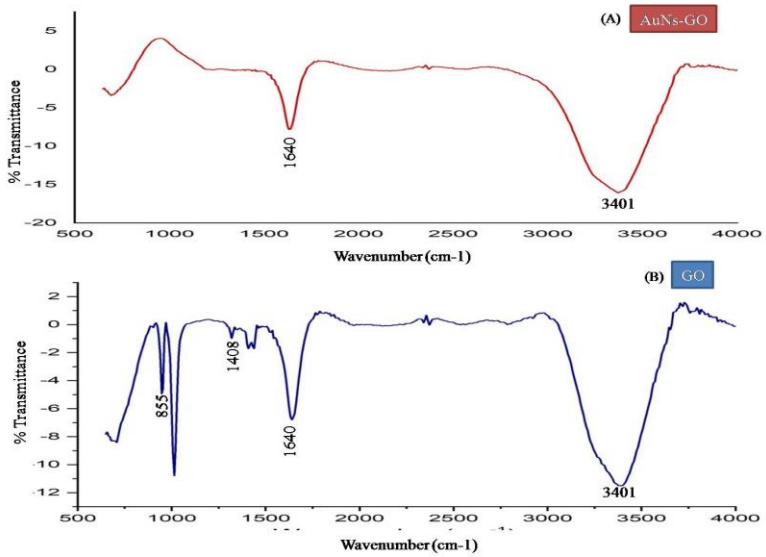

Figure 3. FTIR spectra of (A) AuNs-GO and (B) GO in a range of 500-4000 cm^{-1}.

3.1.3. DLS (Dynamic light scattering).

In Au modified GO particle size and size distribution were evaluated using a Nano zeta-sizer system (Malvern Instruments) having measurement parameters consisting of a scattering angle of 173° (fixed) and wavelength of 632 nm, having a system measurement temperature of 25°C, a sample viscosity of 0.8872 mPa.s and a sample refractive index (RI) of 1.330, and a material RI of 0.20. Before performing the DLS measurement, the sample volume was passed through a 0.2 µm polyvinylene fluoride membrane (PVDF). Then the sample was loaded into the quartz cuvette, and the measurement was performed by DLS studies.The size of 76.72 nm with a Pdl of 0.621 (Figure 4) enumerates the achievement of Au modified GO.

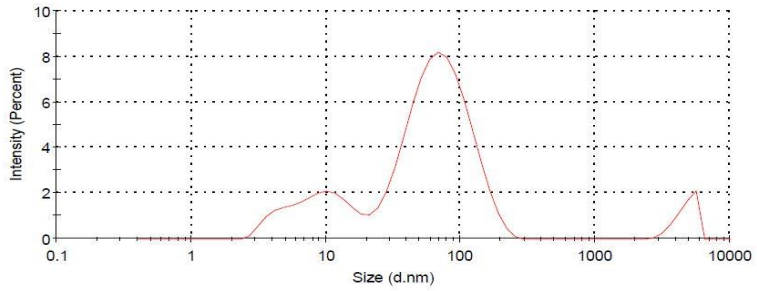

Figure 4. Size distributions of Au nanoparticles in prepared Au Modified GO measured by the DLS technique.

3.1.4. Field-Emission Scanning Electron Microscopy-FE-SEM).

Further, the AuNs-GO/SPPE sensor was also distinguished using FE-SEM to assure the deposition of AuNs-GO onto the working surface of the electrode surface and immobilization of the DNA probe. The comparison of the working surface area of SPPE at different phases is shown in Figure 5. Figure 5a corresponds to the bare SPPE having carbon as a working surface area which appears as a granular carbon particle layer. Figure 5b corresponds to AuNs-GO modified working surface area, which appears as shiny spherical nanoparticles that assures the deposition of nanocomposite onto the SPPE, and Figure 5c corresponds to the fixation of ssDNA $_{probe}$ onto the AuNs-GO modified SPPE, which formed a very thin layer with a thick cloudy structure and change in surface morphology was observed.

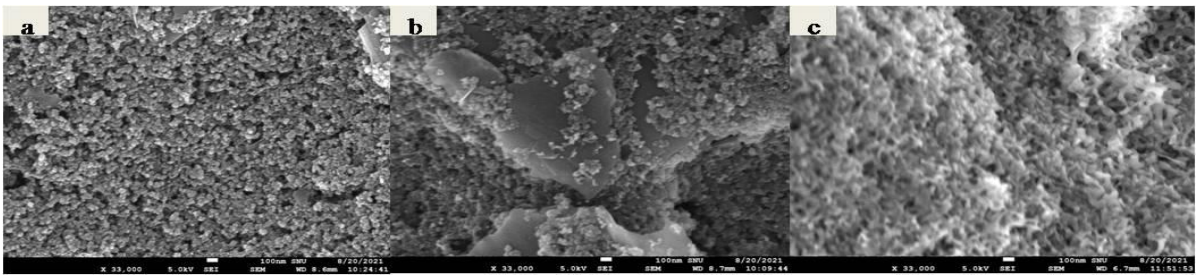

Figure 5. FE-SEM images of (a) showing bare SPPE, (b) showing AuNs-GO modified SPPE, and (c) showing AuNs-GO/SPPE attachment with ssDNA probe. The SEM study was done to ensure the fabrication steps of the DNA sensor.

3.2. Electrochemical characterization (CV and EIS)

3.2.1. Cyclic Voltammetry (CV).

The CV study of the developed DNA sensor shows a linear response with a substantial range of *L. interrogans* ssGDNA dilutions (Figure 6). The CV response was reported before and after immobilization of the *Lipl-41* gene-specific 5'NH_2 labeled, confined $ssDNA_{probe}$ onto

the working area of modified SPPE using 1mM methylene blue (MB) dye prepared in phosphate-buffered saline (PBS) (pH 7.2).

An increase in current value (Ip) was observed after immobilization of the probe, which is due to the addition of guanine bases (DNA) present on the electrode surface that binds with the MB molecules and brings them into the propinquity of the electrode surface resulting in increased electron transfer dynamics. The hybridization of ssDNA probe with different dilutions (0.008-4.2 ng/µl) of ssGDNA of *L. interrogans* that results in an increased guanine base onto the electrode surface equally enhanced the electron shifting rate and the sensor response in terms of (Ip) values. The sensor was reported with a limit of detection (LOD) of 0.002 ng/µl using a standard calibration curve is shown in inset II of Figure 7.The sensor shows a linear response with different dilutions of ssGDNA of *L. interrogans* with a regression coefficient (R^2) of 0.959. The sensibility of the developed DNA biosensor was calculated as 1487.4 µA/cm^2/ng for ssGDNA of *L. interrogans* using CV studies. The linear response of the developed sensor with ssGDNA concentrations confirms the legitimateness of the hybridization phenomena onto the electrode surface. The sensor response was inscribed in triplicates, and all values were plotted by picking the average values.

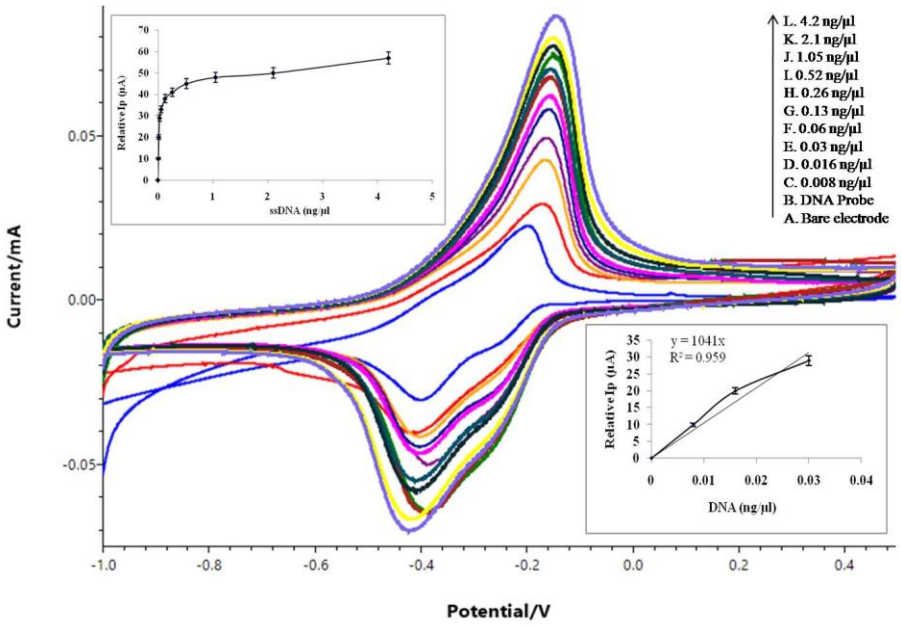

Figure 6. CV investigation of the developed DNA sensor at various junctures of the construction, including (A) the AuNs/SPPE bare electrode, (B) AuNs/SPPE/ssDNA $_{probe}$, and (C–L) hybridization with different concentrations of ssGDNA of *L. interrogans*. Inset I shows a linear calibration curve for the enumeration of the LOD, and inset II exhibits a hyperbolic plot among the Ip values in respect of probe with various dilutions of hybridizing *L. interrogans* ssGDNA.

3.2.2. Impedimetric spectroscopy (IS).

The DNA sensor was further characterized by operating the EIS method using 2.5 mM of potassium ferricyanide in a PBS buffer (pH 7.2) with a frequency band of 1e-^{7} MHz to 0.1MHz. The rise in Rct value was observed upon hybridization with multiple concentrations of *L. interrogans* ssGDNA (20 ng/µl and 40 ng/µl). This is due to the enumeration of the phosphate group present on the electrode surface. So, EIS studies ensure the steps involved in the modification of the SPPE and confirm the hybridization event that occurred on the working area of the electrode surface. The EIS in Figure 7 shows the modification steps of SPPE and the hybridization event recorded with the ssGDNA of *L. interrogans.*

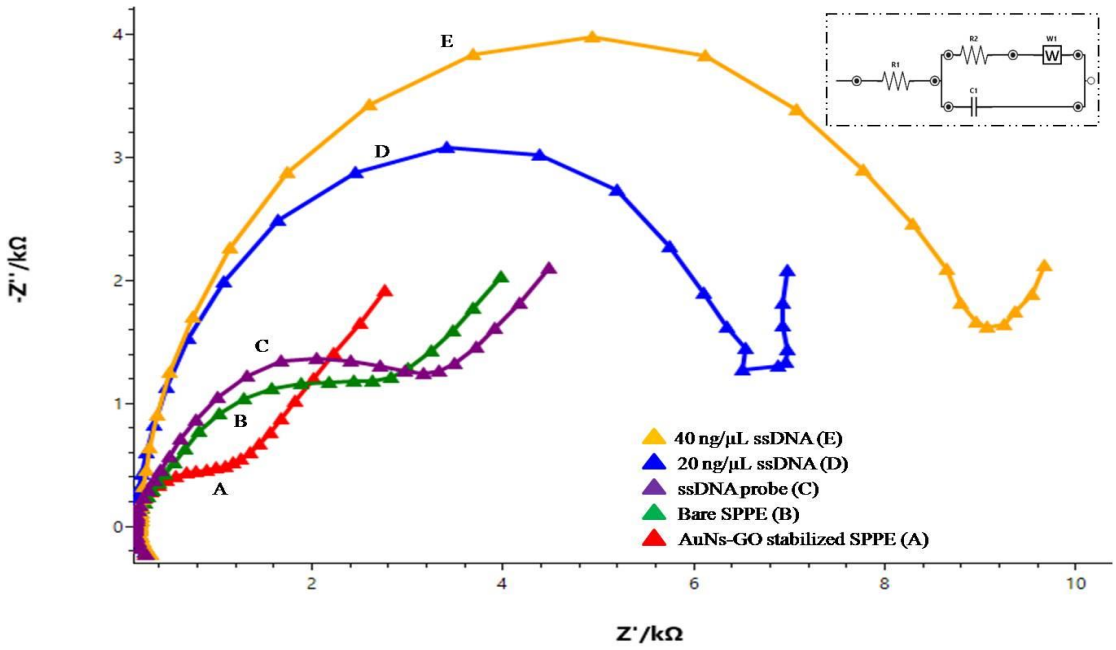

Figure. 7 Evaluation of the electrochemical impedimetric spectrum (EIS) of the developed DNA sensor at different steps, including (A) graphene oxide, stabilized gold nanoparticles, (B) Bare SPPE electrode (C) immobilization of the single-stranded amino-linked ('5') DNA probe, and (D-E) hybridizing with different dilutions of *L. interrogans* ssDNA using 2.5 mM $C_6N_6FeK_3$ solution.

3.2.3. Specificity and selectivity study.

The developed DNA sensor was found to be highly specific for the complementary ssGDNA. The change in relative current (Ip) value in respect of the probe was found higher only after hybridizing with ssGDNA of *L. interrogans* (Figure 8). The other bacterial genomic DNA samples (*E. coli, S. aureus, and O.tsutsugamushi*) and NC (Human G-DNA) show considerable changes in the relative current values after hybridization with the ssDNA probe. The developed DNA sensor can distinguish between the target DNA sequence with the non-complementary DNA sequences, which makes it a masterful tool in diagnosing *L. interrogans* with greater specificity in the suffering patient's blood samples.

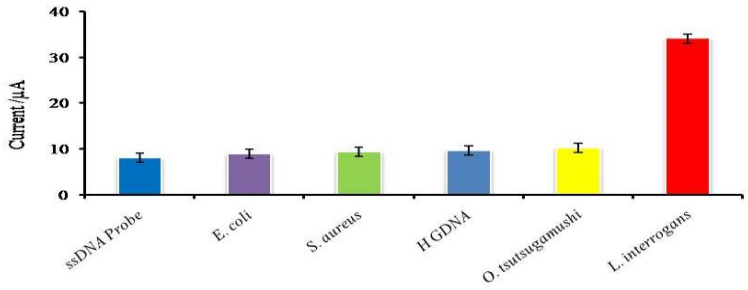

Figure 8. The developed DNA biosensor specialty was assessed with *L. interrogans* and different microorganisms (*S. aureus, E. coli, O.tsutsugamushi*) using CV studies (NC= Human G-DNA).

The DNA probe resilience for the complementary single-stranded GDNA of *L. interrogans* was estimated using the selectivity study (Figure 9). The developed DNA sensor shows higher *Ip* values in respect of the probe with the complementary DNA sequence. A fall in *Ip* values was recorded after hybridization with cDNA sequences and sequences containing a different number of mismatch bases viz. 1-base, 2-base, 3-base, 4-base, and multiple base

mismatch sequences. After hybridization with multiple-bases mismatched DNA sequences, the Ip values were equivalent to none of the probe, which shows negligible changes in current values for the non-complimentary DNA sequences.

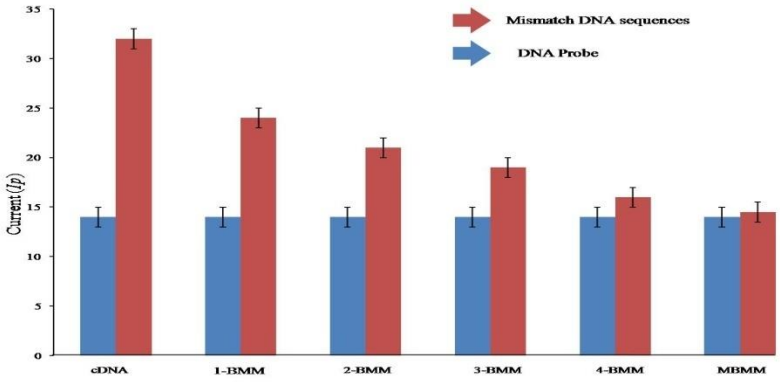

Figure 9. Selectivity of the developed DNA sensor regarding the cDNA carrying different no. of mismatch base sequences. The CV current values in respect of DNA probe were studied after hybridization of DNA sensor with complementary DNA and different no. of mismatch sequences including 1-BMM, 2-BMM, 3-BMM, 4-BMM, and (MBMM).

3.2.4. Validation of DNA sensor.

The noticeable changes in peak current (*IP*) values (Figure 10) were only observed in 10 samples and the positive control samples after the hybridization of ssGDNA with the specific DNA probe. The developed sensor response in terms of CV for the positive control (PC) and Positive samples (Patient's sample) in respect of the probe was found to be higher, and no or negligible response was recorded with the negative control sample (NC). The lower DNA response was observed with the negative sample (NC) due to the non-complementary ssGDNA, which could not bind with that specific DNA probe and was rinsed off during the washing ensue after each hybridization incident. The samples were also confirmed using a microscopic agglutination test (MAT) kit and showed consistent results with the developed DNA biosensor. The specificity of the developed biosensor is mostly contributed by the single-stranded DNA probe specific to the *Lipl-41* gene. This shows 100% homology with the genome of *L. interrogans* and found no homology difference with the other pathogenic and human genome under the sequence alignment tool (BLAST) in NCBI. The observed results were relevant to the specificity study, which shows inconsequential sensor response in connection with negative control (NC) and other bacterial species in correlation to the positive control.

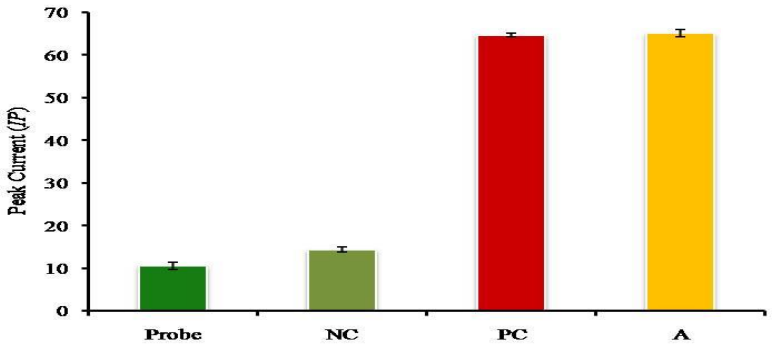

Figure 10. Validation of developed DNA sensor using 10 patients'blood GDNA sample (A), positive control (*L. interrogans* confirmed PCR GDNA samples), and negative control (Human GDNA). The relative peak current concerning the DNA probe through hybridization with the patient's ssGDNA samples was employed for the validation. All assessments were done using a similar concentration of ssGDNA (10 ng/µl) by CV study using 1mM MB dye.

4. Conclusions

The gold nanoparticles-Graphene oxide (AuNs-GO) embedded on SPPE has been demonstrated to be a fine podium for immobilizing specific amine labeled ssDNA probes. The electrochemical detection of the *L. interrogans* marker *Lipl-41* proves to be a great platform that shows a clear signal augmentation cognizable via AuNs and GO. Using the electrochemical detection technique of several dilutions of *L interrogans* ssGDNA, the detection limits (LOD) of 0.002 ng/µL was achieved with a sensibility of 1487.4 µA/cm^2/ng. Thus, the reported developed sensor is better than previously reported sensors in terms of cost, high accuracy, and better endurance and can be used in all remote areas with greater sensitivity and can become an alternative tool for the expeditious stage detection of leptospirosis.

Funding

This research received no external funding.

Acknowledgments

This research has no acknowledgment.

Conflicts of Interest

The authors declare no conflict of interest.

References

1. Budihal, S. V.; Perwez, K. Leptospirosis diagnosis: competancy of various laboratory tests. *J. Clin. Diagn. Res.* **2014**, *8*, 199-202, https://doi.org/10.7860/jcdr/2014/6593.3950.
2. ChaganYasutan,H.; Hanan,F.; Niki,T.; Bai,G.; Ashino,Y.; Egawa,S.; Hattori,T. Plasma osteopontin levels is associated with biochemical markers of kidney injury in patients with leptospirosis. *Diagnostics.* **2020**, *10*, https://doi.org/10.3390/diagnostics10070439.
3. Benschop, J.; Heuer, C.; Jaros, P.; Collins-Emerson, J.; Midwinter, A.; Wilson, P. Seroprevalence of leptospirosis in workers at a NewZealand slaughter house. *N. Z. Med. J.* **2009**,*122*.
4. Desai, S.; vanTreeck, U.; Lierz, M.; Espelage, W.; Zota, L.; Czerwinski, M.; Jansen, A. Resurgence of field fever in a temperate country: an epidemic of leptospirosis among seasonal strawberry harvesters in Germany in 2007.*Clin Infect Dis.* **2009**, *48*, 691-697, https://doi.org/10.1086/597036.
5. Stern, E. J.; Galloway, R.; Shadomy, S. V.; Wannemuehler, K.; Atrubin, D.; Blackmore, C.; Clark, T. A. Outbreak of leptospirosis among Adventure Race participants in Florida, 2005.*Clin. Infect. Dis.* **2010**, *50*, 843-849, https://doi.org/10.1086/650578.
6. Rajendran, R.; Karmakar, S. R.; Garg, V.; Viswanathan, R.; Zaman, K.; Anusree, S. B.; Sharma, S. N. Post Flood Study on the Incidence of Leptospirosis in Alappuzha District of Kerala, India. *J. Commun. Dis. (E-ISSN:2581-351X&P-ISSN:0019-5138)* **2021**, *53*, 127-134.
7. Musso, D.; LaScola, B. Laboratory diagnosis of leptospirosis: a challenge. *J. Microbiol. Immunol. Infect.* **2013**, *46*, 245-252, https://doi.org/10.1016/j.jmii.2013.03.001.
8. Marquez, A.; Djelouadji, Z.; Lattard, V.; Kodjo, A. Overview of laboratory methods to diagnose leptospirosis and to identify and to type leptospires. *Int. Microbiol.* **2017**, *20*, 184-193, https://doi.org/10.2436/20.1501.01.302.
9. Penna, B.; Marassi, C. D.; Libonati, H.; Narduche, L.; Lilenbaum, W.; Bourhy, P. Diagnostic accuracy of an in-house ELISA using the intermediate species Leptospira fainei as antigen for diagnosis of acute leptospirosis in dogs. *Comp. Immunol. Microbiol. Infect. Dis.* **2017**, *50*, 13-15, https://doi.org/10.1016/j.cimid.2016.11.004.
10. Nisansala, G. G. T.; Muthusinghe, D.; Gunasekara, T. D. C. P.; Weerasekera, M. M.; Fernando, S. S. N.; Ranasinghe, K. N. P.; Gamage, C. D. Isolation and characterization of Leptospira interrogans from two patients with leptospirosis in Western Province, SriLanka. *J. Med. Microbiol.* **2018**, *67*, 1249-1252, https://doi.org/10.1099/jmm.0.000800.
11. Perumal, V.; Hashim, U. Advances in biosensors: Principle, architecture and applications. *J. Econ. Financ. Adm. Sci.* **2013**, *12*, 1-15, https://doi.org/10.1016/j.jab.2013.02.001.

12. Kurbanoglu, S.; Erkmen, C.; Uslu, B. Frontiers in electrochemical enzyme based biosensors for food and drug analysis. *Trends Analyt. Chem.* **2020**, *124*, https://doi.org/10.1016/j.trac.2020.115809.
13. Naresh, V.; Lee, N. A review on biosensors and recent development of nano structured materials-enabled biosensors. *Sensors.* **2021**, *21*, https://doi.org/10.3390/s21041109.
14. AlMannai, A.; Haik, Y.; Elmel, A.; Qadri, S.; Saud, K. M. 3D SERS-based biosensor for the selective detection of circulating cancer-derived exosomes. *Emerg. Mater*. **2021**, 1-13, https://doi.org/10.1007/s42247-021-00325-z.
15. Mohammadi, S.; Salimi, A.; Hoseinkhani, Z.; Ghasemi, F.; Mansouri, K. Carbon dots hybrid for dual fluorescent detection of micro RNA-21 integrated bioimaging of MCF-7 using a micro fluidic platform. *J. Nanobiotechnology*. **2022**, *20*, 1-15, https://doi.org/10.1186/s12951-022-01274-3.
16. Wang, L.; Zeng, H.; Yang, X.; Chen, C.; Ou, S. Integrated nicking enzyme-powered numerous-legged DNA walker prepared by rolling circle amplification for fluorescence detection of micro RNA. *Microchim. Acta.* **2021**, *188*, 1-8, https://doi.org/10.1007/s00604-021-04875-1.
17. Białobrzeska, W.; Dziąbowska, K.; Lisowska, M.; Mohtar, M. A.; Muller, P.; Vojtesek, B.; Nidzworski, D. An ultrasensitive biosensor for detection of femtogram levels of the cancer antigen AGR2 using monoclonal antibody modified screen-printed gold electrodes. *Biosensors.* **2021**, *11*, https://doi.org/10.3390/bios11060184.
18. Xu, M.; Zhu, Y.; Gao, S.; Zhang, Z.; Gu, Y.; Liu, X. Reduced graphene oxide-coated silica nanospheres as flexible enzymatic biosensors for detection of glucose in sweat. *ACS Appl. Nano. Mater.* **2021**, *4*, 12442-12452, https://doi.org/10.1021/acsanm.1c02887.
19. Stasyuk, N.; Gayda, G.; Demkiv, O.; Darmohray, L.; Gonchar, M.; Nisnevitch, M. Amperometric biosensors for L-arginine determination based on L-arginine oxidase and peroxidase-like nanozymes. *Appl. Sci.* **2021**, *11*, https://doi.org/10.3390/app11157024.
20. Lopez, A.; Liu, J. Nanomaterial and aptamer-based sensing: target binding versus target adsorption illustrated by the detection of adenosine and ATP on metal oxides and graphene oxide. *Anal. Chem.* **2021**, *93*, 3018-3025, https://doi.org/10.1021/acs.analchem.0c05062.
21. Gosai, A.; Khondakar, K. R.; Ma, X.; Ali, M. Application of Functionalized Graphene Oxide Based Biosensors for Health Monitoring: Simple Graphene Derivatives to 3D Printed Platforms. *Biosensors* **2021**, *11*, https://doi.org/10.3390/bios11100384.
22. Safarzadeh, M.; Suhail, A.; Sethi, J.; Sattar, A.; Jenkins, D.; Pan, G. A Label-free DNA-immuno sensor based on aminated rGO electrode for the quantification of DNA methylation. *Nanomaterials* **2021**, *11*, https://doi.org/10.3390/nano11040985.
23. Gosai, A.; Khondakar, K. R.; Ma, X.; Ali, M. Application of Functionalized Graphene Oxide Based Biosensors for Health Monitoring: Simple Graphene Derivatives to 3D Printed Platforms. *Biosensors* **2021**, *11*, https://doi.org/10.3390/bios11100384.
24. Waiwinya, W.; Putnin, T.; Pimalai, D.; Chawjiraphan, W.; Sathirapongsasuti, N.; Japrung, D. Immobilization free electrochemical sensor coupled with a graphene-oxide-based aptasensor for glycated albumin detection. *Biosensors* **2021**, *11*, https://doi.org/10.3390/bios11030085.
25. Tang, Z.; Wu, H.; Cort, J. R.; Buchko, G. W.; Zhang, Y.; Shao, Y.; Lin, Y. Constraint of DNA on functionalized graphene improves its biostability and specificity. *Small.* **2010**, *6*, 1205-1209, https://doi.org/10.1002/smll.201000024.
26. Wang, Y.; Li, Z.; Wang, J.; Li, J.; Lin, Y. Graphene and graphene oxide: biofunctionalization and applications in biotechnology. *Trends. Biotechnol.* **2011**, *29*, 205-212, https://doi.org/10.1016/j.tibtech.2011.01.008.
27. Shahriari, S.; Sastry, M.; Panjikar, S.; Raman, R. S. Graphene and Graphene Oxide as a Support for Biomolecules in the Development of Biosensors. *Nanotechnol. Sci. Appl.* **2021,** *14*, https://doi.org/10.2147/nsa.s334487.
28. Saha, K.; Agasti, S. S.; Kim, C.; Li, X.; Rotello, V. M. Gold nanoparticles in chemical and biological sensing. *Chem. Rev.* **2012**, *112*, 2739-2779, https://doi.org/10.1021/cr2001178.
29. Huong, V. T.; Phuong, N. T. T.; Tai, N. T.; An, N. T.; Lam, V. D.; Manh, D. H.; Tran, N. H. T. Gold nanoparticles modified a multimode clad-free fiber for ultrasensitive detection of bovine serum albumin. *Nanomaterials.* **2021**, https://doi.org/10.1155/2021/5530709.
30. Dong, Y.; Zhang, T.; Lin, X.; Feng, J.; Luo, F.; Gao, H.; He, Q. Graphene/aptamer probes for small molecule detection: from in vitro test to in situ imaging. *Microchim. Acta.* **2020**, *187*, 1-18, https://doi.org/10.1007/s00604-020-4128-8.
31. Nagraik, R.; Kaushal, A.; Gupta, S.; Sethi, S.; Sharma, A.; Kumar, D. Nanofabricated versatile electrochemical sensor for *Leptospira interrogans* detection. *J. Biosci. Bioeng.* **2020**, *129*, 441-446, https://doi.org/10.1016/j.jbiosc.2019.11.003.
32. Verma, V.; Kala, D.; Gupta, S.; Kumar, H.; Kaushal, A.; Kuča, K.; Kumar, D. Leptospira interrogans outer membrane based nanohybrid sensor for the diagnosis of leptospirosis. *Sensors* **2021**, *21*, https://doi.org/10.3390/s21072552.
33. Shang, E. S.; Summers, T. A.; Haake, D. A. Molecular cloning and sequence analysis of the gene encoding LipL41, a surface-exposed lipoprotein of pathogenic Leptospira species. *Infect. Immun*. **1996**, *64*, 2322-2330, https://doi.org/10.1128/iai.64.6.2322-2330.1996.

34. Golab, N.; Khaki, P.; Harzandi, N.; Esmaelizad, M.; Tebianian, M. Expression and purification of the Lipl41, a surface-exposed lipoprotein antigen of pathogenic Leptospira spp. *Vet. Arh.* **2020**, *90*, 297-305, https://doi.org/10.24099/vet.arhiv.0803.
35. Nagraik, R.; Sethi, S.; Sharma, A.; Kumar, D.; Kumar, D.; Kumar, A. P. Ultrasensitive nanohybrid electrochemical sensor to detect LipL32 gene of *Leptospira interrogans*. *Chem. Pap.* **2021**, *75*, 5453-5462, https://doi.org/10.1007/s11696-021-01737-1.
36. Kala, D.; Sharma, T. K.; Gupta, S.; Nagraik, R.; Verma, V.; Thakur, A.; Kaushal, A. AuNPs/CNF-modified DNA biosensor for early and quick detection of *O. tsutsugamushi* in patients suffering from scrub typhus. *3Biotech*. **2020a**, *10*, 1-13, https://doi.org/10.1007/s13205-020-02432-w.
37. Kala, D.; Gupta, S.; Nagraik, R.; Verma, V.; Thakur, A.; Kaushal, A. Diagnosis of scrub typhus: recent advancements and challenges. *3Biotech*. **2020b**, *10*, 1-21, https://doi.org/10.1007/s13205-020-02389-w.
38. Verma, V.; Goyal, M.; Kala, D.; Gupta, S.; Kumar, D.; Kaushal, A. Recent advances in the diagnosis of leptospirosis. *Front. Biosci*. **2020**, *25*, 1655-1681, https://doi.org/10.2741/4872.
39. Song, J.; Xu, L.; Xing, R.; Li, Q.; Zhou, C.; Liu, D.; Song, H. Synthesis of Au/graphene oxide composites for selective and sensitive electrochemical detection of ascorbic acid. *Sci. Rep.* **2014**, *4*, 1-7, https://doi.org/10.1038/srep07515.
40. Chen, J.; Yao, B.; Li, C.; Shi, G. An improved Hummers method for eco-friendly synthesis of graphene oxide. *Carbon*. **2013**, *64*, 225-229, https://doi.org/10.1016/j.carbon.2013.07.055.
41. Marcano, D. C.; Kosynkin, D. V.; Berlin, J. M.; Sinitskii, A.; Sun, Z.; Slesarev, A.; Tour, J. M. Improved synthesis of graphene oxide. *ACS nano.* **2010**, *4*, 4806-4814, https://doi.org/10.1021/nn1006368.
42. Yang, X.; Ma, L.; Wang, S.; Li, Y.; Tu, Y.; Zhu, X. "Clicking" graphite oxide sheets with well-defined polystyrenes: a new strategy to control the layer thickness. *Polymer*. **2011**, *52*, 3046-3052, https://doi.org/10.1016/j.polymer.2011.04.062.
43. Toh, S. Y.; Loh, K. S.; Kamarudin, S. K.; Daud, W. R. W. Graphene production via electrochemical reduction of graphene oxide: Synthesis and characterisation. *Chem. Eng. J.* **2014**, *251*, 422-434, https://doi.org/10.1016/j.cej.2014.04.004.